UC Merced

UC Merced Previously Published Works

Title

Coupling of Rhythms in Prefrontal Cortex and Autonomic Nervous System in School-Age Children

Permalink

https://escholarship.org/uc/item/0m0288gd

Journal

Annals of the New York Academy of Sciences, 1555(1)

ISSN

0077-8923

Authors

Steffen, Grace

Lindig, Katherine

Howard, Cullin J

et al.

Publication Date

2026

DOI

10.1111/nyas.70203

Peer reviewed

eScholarship.org Powered by the California Digital Library
University of California

Annals of the New York Academy of Sciences

ANNALS OF THE NEW YORK ACADEMY OF SCIENCES

ORIGINAL ARTICLE OPEN ACCESS

Coupling of Rhythms in Prefrontal Cortex and Autonomic Nervous System in School-Age Children

Grace Steffen[1] | Katherine Lindig[1] | Cullin J. Howard[1] | Christian Jerry[1] | Christopher Bell[1] | Kayley E. Morrow[1] | Daisy Gallegos[1] | Assaf Oshri[1] | Cynthia Suveg[1] | Christopher Kello[2] | Drew H. Abney[1]

[1]University of Georgia, Athens, Georgia, USA | [2]University of California Merced, Merced, California, USA

Correspondence: Grace Steffen (grace.steffen@uga.edu)

Received: 2 August 2025 | **Revised:** 23 December 2025 | **Accepted:** 24 December 2025

Keywords: continuous wavelet coherence (CWC) | functional near-infrared spectroscopy (fNIRS) | heart-brain rhythms | neurophysiological coupling | respiratory sinus arrhythmia (RSA) | stress | temporal dynamics

ABSTRACT

Self-regulation is a neuroregulatory process driven by function in both the autonomic nervous system (ANS) and dorsolateral prefrontal cortex (dlPFC). Although many investigations have explored the role of these systems in self-regulation independently, little work has examined how they cooperate across contexts, limiting the understanding of neurophysiological substrates of self-regulation. In a sample of 55 children ($M_{age} = 5.85$, $SD = 0.80$), the present study examined the coordination of cardiac and neural signals during rest and a mildly stressful task. Paired-samples *t*-tests confirmed that the stressor elicited increases in heart rate (HR) and decreases in respiratory sinus arrhythmia (RSA), while correlations indicated stability in individual differences across phases. Wavelet transform coherence assessed coupling of dlPFC signals with HR and RSA. HR– and RSA–dlPFC coupling was observed in both contexts, but timescales of significant coupling varied across contexts, cardiac signals, and dlPFC hemispheres. No associations were found between the coupling of any signal at any timescale and child positive or negative affect or emotion regulation dysfunction. Findings suggest that cardiac–neural coupling is sensitive to timescale, context, and choice of cardiac signal. Future studies should consider other measures of behavioral regulation to better understand its potential relation with ANS–dlPFC coupling.

1 | Introduction

Early childhood is a crucial period for the development of self-regulation—the ability to manage thoughts, emotions, and behaviors to pursue goals and adapt to various situations [1]. At this age, children begin to apply regulatory strategies developed alongside caregivers to new settings [2, 3]. Biological systems underlie self-regulation processes; many of which undergo significant maturation during early childhood [4]. Thus, much research aims to understand these systems during early childhood, with a specific focus on the role of different neurophysiological markers of regulation. These markers usually fall into two categories: cardiac indices of autonomic nervous system (ANS) functioning (e.g., heart rate [HR] and respiratory sinus arrhythmia [RSA]), and neural markers of central nervous system functioning indexed by various neuroimaging techniques, such as functional magnetic resonance imaging (fMRI) and functional near-infrared spectroscopy (fNIRS).

The ability to flexibly respond and recover from stressors using the ANS is a biomarker of effective self-regulation [5, 6]. The ANS is a socially responsive neuroregulatory system that coordinates the body's response to environmental challenges by regulating physiological processes in an effort to maintain homeostasis [7, 8]. Under the direction of the central autonomic network (CAN), the ANS modulates physiological arousal through its sympathetic

This is an open access article under the terms of the Creative Commons Attribution-NonCommercial License, which permits use, distribution and reproduction in any medium, provided the original work is properly cited and is not used for commercial purposes.

© 2026 The Author(s). *Annals of the New York Academy of Sciences* published by Wiley Periodicals LLC on behalf of The New York Academy of Sciences.

and parasympathetic branches [9, 10]. The sympathetic nervous system (SNS) increases HR and redirects blood flow through vasoconstriction, acting on target organs via preganglionic neurons in the lateral horn of the spinal cord that synapse on ganglia near proximal vertebral segments [11]. Compared to the SNS, the parasympathetic nervous system (PNS) is a relatively faster-acting system that promotes restorative functions and modulates HR and vasodilation through the myelinated ventral vagus nerve [12, 13]. Although the SNS maintains some level of daily engagement, the PNS is the primary mediator of physiological regulation for normative daily stressors [11, 14, 15]. In coordination with the ANS, the baroreceptor reflex is a CAN-influenced compensatory mechanism that maintains stable blood pressure and HR by modulating autonomic outflow in response to changes in arterial stretch [11]. Because the ANS continuously modulates HR, blood pressure, and respiration to match internal demands with external conditions, cardiac activity is a particularly effective measure of ANS function [5].

HR and RSA are complementary cardiac indices of autonomic functioning that reflect different aspects of regulatory control. HR, the number of heart beats occurring in a given period, serves as a broad indicator of physiological arousal resulting from multiple bioregulatory influences, including sympathetic and parasympathetic activity, respiration, and baroreflex mechanisms [16]. In contrast, RSA reflects beat-to-beat variability in HR that occurs at the frequency of spontaneous respiration (i.e., high-frequency heart rate variability [HRV]) and is widely interpreted as an index of parasympathetic control over physiological arousal mediated by the ventral vagus nerve [17]. Accordingly, RSA is considered an indirect index of vagal activity, a fundamental bidirectional brain–body communication system [17, 18]. Whereas high HR indicates elevated arousal, high RSA signals a deceleration of HR brought about through greater vagal influence over the cardiac sinoatrial node. Low resting RSA and disproportionately high or low RSA reactivity during challenging and/or emotional tasks have been associated with poor self-regulatory skills in both adults and children [6, 19]. Likewise, higher or sustained HR during stress tasks is associated with heightened physiological arousal, which is indicative of a reduced capacity to engage with stressors and flexibly recover, a pattern linked to poorer emotional and behavioral regulation. Thus, RSA signals faster changes in cardiac activity thought to stem from PNS involvement, while HR characterizes slower cardiac changes that may stem from a more diverse set of other autonomic sources.

The prefrontal cortex (PFC) is involved in high-level cognitive functions that support self-regulation [20, 21]. This brain area develops later in life relative to other cortical regions [22, 23]. Moreover, children exhibit decreased resting-state connectivity in the PFC compared to adults [24–26]. Disruptions in prefrontal resting-state fMRI have been related to early life stress [27], and decreased connectivity between the medial prefrontal cortex and amygdala has been related to aggressive behaviors and adverse experiences in 4- to 7-year-old children [28]. Conversely, increased activity in the lateral PFC during a stressful task has been related to increased emotion regulation capacity in children aged 4–6 [29]. Such differences in the association between PFC and self-regulation in children as compared to adults suggest that the ability to self-regulate develops alongside the PFC [30].

Early childhood has been postulated to be a salient period for both the development of self-regulation and the PFC. Significant changes in the structural architecture of the PFC occur during this period, including a rapid decline in synaptogenesis, increases in cortical thickness, and increases in gray and white matter [31]. These changes have been related to the development of cognitive function associated with the PFC, such as increased performance on cognitive tasks targeting inhibitory control [32–36] and working memory [37]. This period is also marked by notable increases in self-regulation and broader executive functioning [38]. These changes are facilitated by the interaction between concurrent neurophysiological development and environmental changes that accompany this transitional period [39]. These environmental changes include social hierarchies and increased participation in responsibilities in the home and at school [38, 39]. Studies focusing on the dorsolateral PFC (dlPFC) in particular suggest it plays an integral role in cognitive control and behavioral adaptation in the face of challenge or conflict, which are key components of self-regulation [40–42]. More specifically, irritability in childhood has been associated with decreases in dlPFC activity in response to maternal criticism in adolescence [43]. Increases in dlPFC activity have also been associated with decreased behavioral aggression across middle and late childhood [44]. Examining the temporal response of the dlPFC to challenges during the early middle childhood period may increase the understanding of how and why PFC activity has been related with behavioral regulation.

While there are large bodies of work exploring the roles of the PFC and cardiac physiology in self-regulation independently, less work has examined how these signals may be related to one another. These separate bodies of work suggest that both physiological systems play a fundamental role in self-regulation, particularly during development. Neurobiological models of the stress system describe the interaction between the PFC and ANS in the face of stress as a series of feedback loops, in which ANS response is mediated by and interacts with various systems, predominantly neural circuits, including the PFC, which in turn modulate behavioral responses to stress [45].

The relation between these systems in other contexts remains less clear. However, both the PFC and ANS are active at rest, and indices of their activity at rest are associated with self-regulation ability and psychopathology [6]. More broadly, the neurovisceral integration model suggests that the mechanism through which the PFC, alongside other regions such as the orbitofrontal cortex and anterior cingulate cortex, is involved in self-regulation is through regulation of the ANS via the top-down control these regions exert over subcortical and brainstem structures [6, 45, 46]. More recently, this model has posited that RSA captures peripheral or downstream PFC function, supported by associations between executive function task performance and resting RSA, and between RSA and PFC activity [6]. Preliminary evidence suggests that levels of resting RSA are positively associated with PFC activation [9, 46]. Concerning untransformed HR, transcranial stimulation of the PFC has been associated with significant decreases in HR in adults with major depressive disorder [47] and in autistic children and young adults aged 7–21 years old [48].

However, most studies examining links between these two systems have done so by indexing the amount of activity in these signals across the duration of tasks (e.g., emotion- and stress-eliciting tasks vs. at rest) [46]. For example, a meta-analysis examining associations between HRV and brain activity in adults [46] included studies that use such methods, and results suggest that there is a positive association between HRV and PFC activity, particularly during emotion-eliciting tasks [46]. Although these findings are informative, this method for examining associations between cardiac and neural activity does not provide insight into whether these two signals are indexing some common signal, with RSA capturing downstream PFC activity [6], or if these signals interact in unique, independent ways that converge over time to produce a cohesive response to external stimuli when studied at a broader timescale. The temporal coupling between these systems remains understudied because the difference in timescales at which these processes are carried out is very challenging from an analytic perspective. Previous research has used cross-recurrence quantification analysis [49] to examine coupling between PFC and RSA in infants and their mothers and found no relationship. The authors suggest that these findings may be due in part to their choice of analytic tool, as cross-recurrence analysis was not able to capture fluctuations that occur at multiple timescales. Continuous wavelet coherence may better capture interactions between these signals, as it is nonparametric, normalized, and capable of detecting associations across various timescales while accounting for consistent phase differences that may be produced by a signal that consistently leads or lags another [50]. Understanding how the ANS and PFC coordinate over time at rest and in response to a mildly stressful, naturalistic challenge task could further elucidate such associations.

This study aims to better understand how the ANS and dlPFC interact in young children through physiological and behavioral rhythms to shape self-regulation using a wavelet-based measure of coupling designed to capture the hypothesized timescales of interaction. To gain insight into the relation between coupling, if observed, and behavioral regulation, the association between coherence and children's expression of positive and negative affect throughout the stressor phase is tested. Although studies have traditionally favored the use of RSA to study cardiac physiology and heart–brain interaction in the context of self-regulation, critiques of the conceptualization of RSA have suggested that this signal is not as straightforward as previous work has posited [51]. Therefore, this study will also examine the coupling between the untransformed HR data and dlPFC activity, thereby allowing for the exploration of lower-frequency oscillations in ANS activity in this neuroregulatory process.

While the aim of this study is primarily exploratory, some hypotheses are formulated about the signals and timescales where coupling will be found. First, it is predicted that increases and decreases in dlPFC activity will be related to increases and decreases in cardiac activity (both HR and RSA) during both rest and stressor phases and reflected in coherence values higher for true compared to random pairings, regardless of timescale. The relationship is expected to be observed in timescales related to respiratory cardiac physiology (3–5 s) for dlPFC–HR coupling and in longer timescales around 31–33 s in dlPFC–RSA coupling, given the support for 30-s timescales in most RSA literature. Previous studies have suggested that self-regulation is lateralized within the dlPFC, with activation of the right dlPFC being more sensitive to verbal content, and left dlPFC being more sensitive to nonverbal and affective content [52, 53]. Therefore, it is expected that stronger associations between coupling and positive and negative affect will be observed for the left dlPFC. Comparing dlPFC coupling with both RSA and HR will capture a broader picture of the interaction between cardiac and neural systems. It may also further tease apart the information that RSA signals can provide that untransformed HR data does not.

2 | Methods

2.1 | Participants

Eighty mother–child dyads were included in the full sample. Only children were included in the present analysis. Twenty-five children were excluded from analyses due to incomplete physiological data or technical issues (e.g., optodes or electrodes coming loose, noisy physiological signals) during data collection, resulting in a final sample of 55 children ($M_{age} = 5.85$, $SD = 0.80$; 56.5% females). Children were required to be between the ages of 5 and 7 years old and have no developmental concerns that could prevent completion of study procedures. Families were required to speak English. Half (50.0%) of children were White, 28.8% Black or African American, and 21.2% were specified as other races. Regarding children's ethnicity, about 10% of mothers indicated their children were of Hispanic, Latinx, or Spanish heritage. Mothers reported completing a bachelor's degree (32.5%), a graduate degree (37.5%), some college (23.80%), a high school diploma (3.8%), and 2.6% reported having less than a high school diploma. A majority of mothers were currently employed (76.9%). Regarding annual family income, approximately 11.5% of the families were lower than $29,999, 26.9% between $30,000 and $59,999, 40.4% between $60,000 and $99,999, and 21.2% over $100,000.

2.2 | Procedures

Written informed consent and assent were obtained in-person from mothers and children, respectively, before initiating study procedures. All study procedures were approved and in accordance with the university's Institutional Review Board (PROJECT00004285). Before beginning the experiment, research staff fitted both the child and the mother with electrodes and electroencephalography caps. Dyads were then instructed to watch a 2-min video of calming nature scenery (i.e., resting phase) while cardiac physiology and fNIRS data were collected continuously. Dyads then engaged in a 5-min mild stressor phase in which children were asked to build a LEGO figure to receive a prize. Parents were told they could verbally, but not physically, assist the child. To induce mild stress, several features were implemented based on prior work [54–56]. First, the LEGO figure was beyond the developmental ability of 5- to 7-year-olds and did not include all the pieces needed to construct the figure. Second, children were informed that the task was easy and that "even little kids finish on time." Third, an iPad was placed in front of the dyad that showed a 5-min timer. An automated voice announced how much time was left at each minute. This task has been used to successfully induce mild stress in previous

studies [57, 58]. Video recordings, cardiac physiology, and neural physiology were collected continuously throughout the study. Video recordings were later micro-coded for individual mother and child positive affect (PA) and negative affect (NA). Although physiology signals were collected and behavioral coding was conducted for both mothers and children, only child measures are used for the present study. Families were compensated $100 for participation and $20 for each referral provided.

2.3 | Measures

2.3.1 | Cardiac Physiology

Participants were outfitted with noninvasive electrodes connected to a BIOPAC wireless electrocardiogram (ECG) transmitter belt to monitor cardiac physiology (ECG) throughout the study. The belt transmitted data at a sampling rate of 2 KHz to a BIOPAC MP160 system, which was recorded using BIOPAC's software AcqKnowledge. Electrodes were placed on each parent's and child's bodies following the BIOPAC modified Lead II procedure: ground and VIN+ electrodes were on the participants' stomach above the belly button on the left and right side, while VIN− electrodes were placed below the left collarbone (BIOPAC, Santa Barbara, CA, USA). Research assistants tested the strength of the signal and adjusted it accordingly before starting the study. Interbeat intervals (IBIs) were extracted offline, and artifacts were removed by trained research assistants using CardioEdit (*V6*) software (Brain Body Center, University of Illinois at Chicago). To extract RSA in children aged 5–7 years, a bandpass filter of 0.3–1.3 Hz was used. The lower bound follows the respiratory frequency provided by Wallis and colleagues [59] for the present study's age group and ensures that slower, nonrespiratory HR fluctuations (e.g., drift, Mayer waves) are excluded. The upper bound is higher than the respiratory frequency provided by Wallis et al., and the typical 1.04 Hz used in other studies [60]. However, this higher upper bound accommodates faster breathing rates that may occur due to excitement, stress, or mild movement that may be induced by the stressor phase's LEGO task. Further, other work has suggested that including broader frequency bands may help capture additional variation while still correlating well with narrower bands [61, 62].

Data were manually cleaned by trained research assistants, and IBI series were resampled at 1 Hz using linear interpolation in MATLAB to address values missing due to artifact removal. Resampled IBIs were used to calculate HR in beats per minute. The resampled IBI series were then detrended using a symmetric polynomial filter to remove slow, nonstationary trends (e.g., movement-induced baseline shifts, slow drifts in HR [17]). Manual artifact removal and polynomial detrending helped ensure that physiological artifacts in our frequency range were reduced before bandpass filters were applied. A continuous measure of RSA was then calculated by computing the natural log of the variance within a 15-s sliding window [63].

2.3.2 | fNIRS

The NIRSport 16-16 (NIRx Medizintechnik GmbH, Germany) fNIRS system was used to collect oxygenated (HbO) and deoxygenated (HbR) hemoglobin concentration changes in mother–child dyads. The dyads were fitted with ready-made fNIRS caps provided by NIRx with a 10–20 structure. In each probe set, there were eight sources and eight detectors (total = 18 channels) for both the mother and child. The distance between each optode was 3 cm for the child and 5 cm for the mother.

Processing was adapted from instructions provided by Nguyen and colleagues [49]. First, missing values (NaNs) arising from signal issues, movement, and study interruptions were calculated to identify how much missing data belonged to each channel. Linear interpolation was used in MATLAB when necessary to replace missing data with an average of its neighboring data points. Next, visual inspections were completed for each channel, and channels showing severe signal issues and/or motion artifacts were removed. Motion artifacts were identified in HOMER3 [64, 65] when a signal change exceeded a standard deviation threshold of 10 or an amplitude threshold of 0.4, with a 1-s window before and after each detected artifact. An automated process called "channel pruning" was then used in HOMER3 [64, 65] to further identify unusable channels using predefined signal quality and sensor distance criteria. Fifty-five of the original 80 dyads were considered usable for further analysis. Only participants whose 18 channels were all usable were included, resulting in 1980 total channels analyzed across 55 dyads (55 dyads × 2 participants × 18 channels) and 68.80% usable data from the total possible dataset. The 25 (33.20%) excluded subjects were removed due to poor signal-to-noise ratio, excessive motion artifacts, or study interruptions. Afterward, a bandpass filter (0.01−0.2 Hz) was applied to remove irrelevant changes caused by low-frequency drift and high-frequency noise. The cleaned and filtered data were then converted into concentrations of oxyhemoglobin (HbO) and deoxyhemoglobin (HbR), and down-sampled from 7.81 to 1 Hz to match behavioral and ECG data. Only HbR concentrations were included in further analyses, as these signals are less susceptible to neural physiological noise and are considered to have higher spatial precision as compared to HbO [66, 67]. The mean of the activity across the component channels of the left and right dlPFC was used to get an aggregate signal across these areas. The left dlPFC consisted of channels 7, 8, 15, and 16, which connect optodes placed over Fp1, AF3, AF7, and F5. The right dlPFC probes consisted of channels 9, 10, 17, and 18, which connect optodes placed over Fp2, AF4, AF8, and F6 (see Figure 1).

2.3.3 | Behavioral Observations

Behavioral observation codes were adapted from the NICHD Study of Early Child Care and Youth Development Parent-Child Interaction Scales in Middle Childhood [68]. Research assistants received reliability training from the principal investigators. Once research assistants were considered reliable following training, interrater reliability was assessed using the intraclass correlation coefficient (ICC). Coders were each assigned batches of 10 files, from which three files were randomly selected for reliability. Files were required to achieve a reliability score of at least 75%. If a file did not meet this threshold, a consensus file was created through discussion among the coders, and an additional file was selected for reassessment to ensure reliability standards were met.

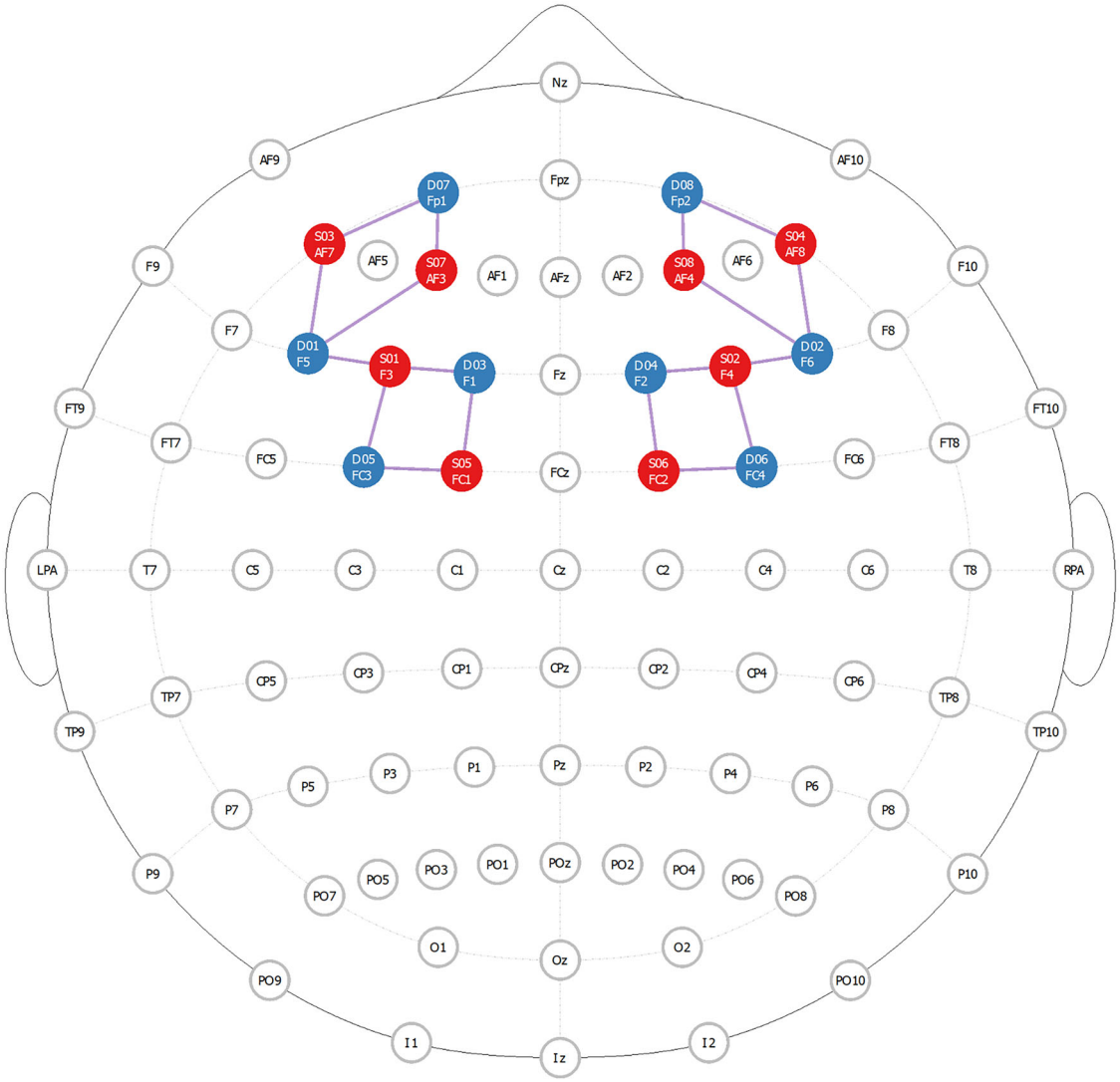


FIGURE 1 | FNIRS montage layout. Red dots indicate source optodes, and blue dots indicate detector optodes. The purple lines connecting sources and detectors are channels.

2.3.4 | Positive Affect

PA was coded individually for the mother and child and was marked by the individuals' expressed positive emotions (e.g., pleasure, enjoyment, happiness) evidenced through animation, smiling, laughter, body posture, and/or tone of voice. PA was captured via the onset and offset of the expressed affect for every second of the 5-min stressor phase. Strong interrater reliability was established for both the onset and offset of PA in children (*ICC* = 0.92).

2.3.5 | Negative Affect

NA captured the individuals' negative emotion (e.g., anger/frustration, sadness, fear, disgust) demonstrated through verbal and facial expressions, body posture, crying, and/or tone of voice. NA was also captured via the onset and offset of the expressed affect in milliseconds across the 5-min stress phase, with excellent interrater reliability across children (*ICC* = 0.96).

To examine associations between PA and NA and ANS–dlPFC coupling, the proportion of time that each was expressed during the task was computed by dividing the number of seconds of each type of affect expression by the total number of seconds in the task (300). Models that included affect used this proportion instead of raw data.

2.3.6 | Children's Emotion Dysregulation

Mothers reported on their child's emotion regulation skills using the Emotion Regulation Checklist Negative Lability (α = 0.80) Subscale [69]. This subscale consists of 15 items, such as "Is easily frustrated,", "Is whiny or clingy with adults," and "Responses angrily to limit-setting by adults" rated on a 4-point Likert scale (1 = *Never* to 4 = *Always*). An average score was calculated across the 15 items and used in analyses. No children were missing questionnaire data.

TABLE 1 | Descriptive statistics of cardiac physiology, brain activity, and affect.

	Resting phase		*Stressor phase*			
Variables	***M***	***SD***	***M***	***SD***	***t*(56)**	***p***
RSA (ln(ms^2))	6.12	1.25	5.22	1.31	7.35	<0.001
HR (bpm)	88.97	13.02	100.04	12.46	−13.75	<0.001
Brain activity (HbR) in right dlPFC (μmol)	−0.02	2.25	0.00	2.88	−1.03	0.308
Brain activity (HbR) in left dlPFC (μmol)	−0.06	2.43	−0.01	2.87	−1.17	0.246
Child positive affect (proportion)	—	—	0.053	0.067	—	—
Child negative affect (proportion)	—	—	0.201	0.145	—	—

Note: Mean and standard deviation of heart rate (HR), respiratory sinus arrhythmia (RSA), deoxygenated hemoglobin (HbR) concentrations, and child affect across the duration of each phase (note that affect was behaviorally coded during the stressor phase only). Decreases in HbR concentrations indicate increased brain activity, such that more negative values indicate more activation on average.

TABLE 2 | Correlations between mean cardiac physiology and brain activity and fixed effects.

	1	**2**	**3**	**4**	**5**	**6**	**7**	**8**	**9**
1. Child age	—								
2. Child resting RSA	0.2	—							
3. Child RSA reactivity	0.09	**0.68*** **	—						
4. Mean left dlPFC activity at rest	−0.11	0.14	0.13	—					
5. Mean right dlPFC activity at rest	−0.06	−0.06	−0.09	0.26*	—				
6. Mean left dlPFC activity during stress	−0.11	0.01	−0.04	0.02	−0.03	—			
7. Mean right dlPFC activity during stress	0	0	−0.04	0.09	**0.62*** **	0.25	—		
8. Child positive affect	0.14	0.14	0.13	0.09	0.05	0.05	0.31*	—	
9. Child negative affect	−0.11	0.14	−0.06	0.15	−0.01	−0.19	−0.38**	−0.32**	—
10. Child emotion dysregulation	−0.04	0.02	−0.02	0.14	0.12	−0.15	0.02	−0.21	0

Note: Correlations in bold remained significant after Bonferroni–Holmes correction. RSA reactivity is the mean RSA value for the duration of the stressor phase. Child emotion dysregulation refers to scores on the ERC Negativity/Lability Subscale.
*** < 0.001, ** < 0.01, * < 0.05.

2.4 | Preliminary and Descriptive Statistics

All preliminary analyses were conducted in R. Participant-level means and standard deviations of each physiological measure (HR, RSA, and dlPFC HbR concentrations) were calculated separately for the resting and stressor phases. Paired-samples *t*-tests were used to compare mean levels of these physiological measures between the resting and stressor phases. Means and standard deviations of the proportion of child positive and negative affect expressed during the stressor phase were also calculated and are reported in Table 1.

Pearson product-moment correlations were computed among physiological measures (resting and stressor phase HR, RSA, and left and right dlPFC HbR activity), behavioral measures (child emotion dysregulation and the proportion of positive and negative affect expression), and child age (Table 2). To control for multiple comparisons, *p*-values were adjusted using the Bonferroni–Holmes correction.

2.5 | HR– and RSA–dlPFC Coupling Analysis

Wavelet transform coherence (WTC) of fNIRS and cardiac physiology (RSA or HR) time-series data was used as estimates of dlPFC–ANS coupling through rhythmic phase relations [50]. WTC was calculated with the *wtc* function from the *biwavelet* package in R [70], using the default Morlet wavelet [71]. To examine the timescale at which this coupling may occur, coherence values were extracted at several frequency bands, starting around the frequency of respiration (0.2–0.33 Hz) and halving down to 0.03–0.032 Hz for the resting phase and 0.015–0.016 Hz for the stressor phase, as these reflect the lowest frequencies that could be examined with the amount of time included in each phase (2 and 5 min, respectively). These bands were chosen so that neural coupling with both respiratory and nonrespiratory cardiac rhythms, such as Mayer waves and baroreflex activity, could be examined. To determine whether there is meaningful variability in coherence across these timescales, a band was extracted across all timescales (3–65 s, or 0.015–0.33 Hz for stressor phase; 3–33 s or 0.033–0.33 Hz for resting phase). For ease of interpretation of these frequency bands in the context of interactions through time, the timescales are referred to in periods, such that the frequency bands correspond to 3–5 (0.2–0.33 Hz), 7–9 (0.11–0.14 Hz), 15–17 (0.058–0.067 Hz), 31–33 (0.030–0.032 Hz), 3–33 (0.03–0.2 Hz), 3–65 (0.015–0.2 Hz), and 63–65 s (0.015–0.016 Hz). Given previous evidence that self-regulation is lateralized within the dlPFC, coherence was calculated separately for the left and right dlPFC. Coherence values were averaged across each of these bands for both HR and RSA signals and across all periods of interest, resulting in 44 coherence values for each participant (right and left dlPFC × RSA and HR × 11 bands; five bands for resting phase and six for stressor phase). To avoid boundary effects, the cone of

influence was removed from all analyses. Three oscillations of a timescale are required for coherence estimations [50]. Therefore, the 5-min task has an additional frequency band of 62–65 s that the 2-min task does not.

To empirically compare the resting and stressor phases while considering the impact that differences in their durations may have on coherence values, a second coherence value was calculated for the stressor phase. For this second calculation, a random, consecutive 2-min segment of time was selected from the 5 min of the stressor phase, and coherence between HR/RSA and dlPFC was calculated following the same procedure described above regarding frequency bands used for the resting phase. This was repeated 10 times to ensure different sections of the phase were captured, and the mean coherence value of the 10 randomly selected segments was taken to create a coherence value representative of the stressor phase while adjusting to a shorter length of time.

2.6 | HR– and RSA–dlPFC Coherence Control Analyses and Modeling

To test for the significance of HR– and RSA–dlPFC coherence values above spurious correlations, random pair analyses were conducted in the same region (left or right dlPFC) and cardiac signal type (HR or RSA) with a permutation approach. To that end, the neural time series of each participant was randomly paired with the RSA or HR time series of other participants. One hundred random pairings were created, and coherence between each pairing was calculated at each of the timescales of interest. To statistically compare coherence values between true and random pairings at each temporal scale, generalized linear mixed effects models were fitted using the *glmmTMB* package [72] in R with family = beta and link = logit, given that coherence values range from 0 to 1. In the primary models (Models 1a−2b; Tables S1–S4), logit-transformed coherence values served as the response variable, and fixed effects of Pairing (true vs. surrogate), Brain Area (left vs. right dlPFC), Timescale (3−5 s, 7–9 s, 15–17 s, 31–33 s, 63–65 s, and all [3−65 s]), and all two- and three-way interactions among them.

A random intercept for subject number (1 | SubjectNumber) was added to account for nesting within subjects. Since each timescale was included for each coherence value for each subject, a crossed random effect (1 | SubjectNumber:Timescale) was added. A chi-square goodness of fit test revealed that the crossed random effects structure provided a significantly better fit than nesting within individuals only (1 | SubjectNumber), $\chi^2(1, 57) = 231.26$, $p < 0.001$. As a check, nesting timescales within subjects (1 + SubjectNumber/timescale) was attempted, which did not significantly improve model fit. Thus, the crossed random-intercept specification was retained in all subsequent models.

To examine whether or not coupling was related to behavioral responses to stress, child emotion dysregulation, and the proportion of child positive and negative affect was included in additional models. Given that differences in coherence patterns by timescale were expected, an interaction term was included for affect by timescale (Models 3a−5b; Tables S5–S10). Child age and basal RSA (when applicable) were controlled. Models 6a and 6b (Tables S11 and S12) were constructed to compare coherence values between these phases across timescale and brain area (Phase × Timescale × Brain Area) to examine differences in coupling between the resting and stressor phases. In these models comparing coherence between the two phases, the 2-min segment calculation of coherence during the stressor phase was used to account for differences in coherence stemming from differences in task duration. To probe Timescale-specific differences across true versus random pairings and coherence values between the two phases, Timescale was treated as a categorical factor, and the *emmeans* package [73] was used to extract pairwise contrasts within each level of Timescale and Brain Area. *p*-Values were corrected for multiple comparisons using the Bonferroni−Holmes method ($\alpha = 0.05$) (Tables 3–8). Coefficient estimates on the log-odds scale were back-transformed to probabilities for ease of interpretation. This approach allowed for determination, at each timescale, of whether observed coherence between cardiac physiology and dlPFC activity reliably exceeded that of random pairs, and whether that true–random difference varied by Brain Area or Timescale.

3 | Results

Paired-samples *t*-tests indicated significant phase-related changes in cardiac physiology (Table 1). Specifically, children exhibited higher HR during the stressor phase compared to the resting phase, $t(56) = -13.75$, $p < 0.001$, and lower RSA during the stressor phase relative to rest, $t(56) = 7.35$, $p < 0.001$, consistent with the induction of an autonomic stress response. Mean HbR concentration did not differ across phases ($ps > 0.24$). Descriptive statistics of child positive and negative affect are also reported in Table 1. Zero-order correlations among cardiac, neural, and behavioral variables are reported in Table 2. Resting and stressor phase RSA were strongly positively correlated, $r = 0.68$, $p < 0.001$, indicating relative stability in individual differences in parasympathetic regulation across phases despite mean-level decreases during stress. Similarly, resting and stressor phase right dlPFC activity were positively correlated, $r = 0.62$, $p < 0.001$. Both correlations remained significant following Bonferroni−Holmes correction.

Coherence estimates of true and random pairings were compared during the resting phase for both HR– and RSA–dlPFC coherence (Models 1a and 1b; Tables 3 and 4). A Type II Wald Chi-square test of the models revealed that Timescale was significant ($p < 0.001$), indicating that coherence varied significantly across timescales. Pairing was also statistically significant for both models, indicating that coherence between true pairings was higher than random pairings ($p < 0.001$) across timescales for both HR– and RSA–dlPFC coherence. However, the statistically significant Pairing × Timescale indicated that this relation also differed by timescale. When the timescale-specific differences between true and random pairings were probed in right and left dlPFC, significance was observed for each timescale ($ps < 0.001$) except 3–5 s ($ps \geq 0.21$) for dlPFC–HR coupling. For dlPFC–RSA coupling, true pairings were significantly greater than random for timescales greater than 3–5 s in the right dlPFC and in only timescales greater than 7–9 s for the left dlPFC.

TABLE 3 | Estimated marginal means for true versus random pairings across timescale and brain area for HR–DlPFC coupling during resting phase.

		Random		True						
Brain area	**Timescale**	**Estimate**	**SE**	**Estimate**	**SE**	**Odds ratio**	**SE**	***Z***	***p***	***Adjusted p***
Left dlPFC	3–5 s	0.23	0.01	0.25	0.01	0.91	0.07	−1.25	0.21	0.21
	7–9 s	0.27	0.01	0.34	0.01	0.72	0.05	−4.58	<0.0001	<0.0001
	15–17 s	0.21	0.01	0.35	0.01	0.49	0.04	−9.59	<0.0001	<0.0001
	31–33 s	0.10	0.01	0.45	0.02	0.13	0.01	−23.01	<0.0001	<0.0001
	3–33 s	0.22	0.01	0.32	0.01	0.60	0.04	−6.89	<0.0001	<0.0001
Right dlPFC	3–5 s	0.23	0.01	0.25	0.01	0.89	0.07	−1.52	0.128	0.142
	7–9 s	0.27	0.01	0.32	0.01	0.76	0.05	−3.78	<0.0001	<0.0001
	15–17 s	0.21	0.01	0.33	0.01	0.52	0.04	−8.73	<0.0001	<0.0001
	31–33 s	0.10	0.01	0.39	0.01	0.18	0.02	−19.52	<0.0001	<0.0001
	3–33 s	0.22	0.01	0.31	0.01	0.63	0.05	−6.31	<0.0001	<0.0001

Note: Adjusted *p* values were corrected for multiple comparison using Bonferroni–Holmes.
Abbreviations: dlPFC, dorsolateral prefrontal cortex; HR, heart rate.

TABLE 4 | Estimated marginal means for true versus random pairings across timescale and brain area for RSA–DlPFC coupling during resting phase.

		Random		True						
Brain area	**Timescale**	**Estimate**	**SE**	**Estimate**	**SE**	**Odds ratio**	**SE**	***Z***	***p***	***Adjusted p***
Left dlPFC	3–5 s	0.28	0.01	0.30	0.02	0.90	0.07	−1.27	0.203	0.203
	7–9 s	0.27	0.01	0.30	0.02	0.86	0.07	−1.86	0.062	0.078
	15–17 s	0.18	0.01	0.28	0.01	0.57	0.05	−6.49	<0.0001	<0.0001
	31–33 s	0.09	0.01	0.44	0.02	0.13	0.01	−20.65	<0.0001	<0.0001
	3–33 s	0.24	0.01	0.32	0.02	0.64	0.05	−5.45	<0.0001	<0.0001
Right dlPFC	3–5 s	0.28	0.01	0.30	0.02	0.89	0.07	−1.45	0.147	0.164
	7–9 s	0.26	0.01	0.30	0.02	0.83	0.07	−2.26	0.024	0.034
	15–17 s	0.18	0.01	0.27	0.01	0.58	0.05	−6.24	<0.0001	<0.0001
	31–33 s	0.10	0.01	0.48	0.02	0.13	0.01	−21.05	<0.0001	<0.0001
	3–33 s	0.24	0.01	0.33	0.02	0.64	0.05	−5.62	<0.0001	<0.0001

Note: Adjusted *p* values were corrected for multiple comparison using Bonferroni–Holmes.
Abbreviations: dlPFC, dorsolateral prefrontal cortex; RSA, respiratory sinus arrhythmia.

TABLE 5 | Estimated marginal means for true versus random pairings across timescale and brain area for HR–DlPFC coupling during stressor phase.

		Random		True						
Brain area	**Timescale**	**Estimate**	**SE**	**Estimate**	**SE**	**Odds ratio**	**SE**	***Z***	***p***	***Adjusted p***
Left dlPFC	3–5 s	0.29	0.01	0.3	0.01	0.94	0.06	−0.95	0.341	0.372
	7–9 s	0.32	0.01	0.34	0.01	0.92	0.06	−1.32	0.186	0.223
	15–17 s	0.29	0.01	0.34	0.01	0.79	0.05	−3.62	<0.0001	<0.0001
	31–33 s	0.25	0.01	0.36	0.01	0.57	0.04	−8.27	<0.0001	<0.0001
	63–65 s	0.16	0.01	0.43	0.01	0.26	0.02	−18.37	<0.0001	<0.0001
	3–64 s	0.26	0.01	0.34	0.01	0.68	0.05	−5.81	<0.0001	<0.0001
Right dlPFC	3–5 s	0.29	0.01	0.29	0.01	0.97	0.07	−0.51	0.609	0.610
	7–9 s	0.32	0.01	0.34	0.01	0.88	0.06	−1.91	0.056	0.075
	15–17 s	0.29	0.01	0.36	0.01	0.73	0.05	−4.7	<0.0001	<0.0001
	31–33 s	0.25	0.01	0.38	0.01	0.56	0.04	−8.64	<0.0001	<0.0001
	63–65 s	0.16	0.01	0.4	0.01	0.30	0.02	−16.55	<0.0001	<0.0001
	3–64 s	0.26	0.01	0.33	0.01	0.68	0.05	−5.68	<0.0001	<0.0001

Note: Adjusted *p* values were corrected for multiple comparison using Bonferroni–Holmes.
Abbreviations: dlPFC, dorsolateral prefrontal cortex; HR, heart rate.

TABLE 6 | Estimated marginal means for true versus random pairings across timescale and brain area for RSA–DlPFC coupling during stressor phase.

		Random		True						
Brain area	**Timescale**	**Estimate**	**SE**	**Estimate**	**SE**	**Odds ratio**	**SE**	***Z***	***p***	***Adjusted p***
Left dlPFC	3–5 s	0.31	0.01	0.32	0.01	0.96	0.06	−0.66	0.512	0.512
	7–9 s	0.31	0.01	0.34	0.01	0.88	0.05	−2.19	0.028	0.038
	15–17 s	0.25	0.01	0.29	0.01	0.84	0.05	−2.72	0.007	0.010
	31–33 s	0.25	0.01	0.37	0.01	0.57	0.04	−9.02	<0.0001	<0.0001
	63–65 s	0.17	0.01	0.42	0.01	0.29	0.02	−18.24	<0.0001	<0.0001
	3–64 s	0.26	0.01	0.34	0.01	0.69	0.04	−5.97	<0.0001	<0.0001
Right dlPFC	3–5 s	0.31	0.01	0.32	0.01	0.96	0.06	−0.7	0.482	0.512
	7–9 s	0.31	0.01	0.34	0.01	0.90	0.05	−1.75	0.081	0.097
	15–17 s	0.26	0.01	0.31	0.01	0.78	0.05	−3.99	<0.0001	<0.0001
	31–33 s	0.26	0.01	0.39	0.01	0.55	0.03	−9.59	<0.0001	<0.0001
	63–65 s	0.17	0.01	0.41	0.01	0.30	0.02	−18.07	<0.0001	<0.0001
	3–64 s	0.26	0.01	0.34	0.01	0.69	0.04	−6.03	<0.0001	<0.0001

Note: Adjusted *p* values were corrected for multiple comparison using Bonferroni–Holmes.
Abbreviations: dlPFC, dorsolateral prefrontal cortex; RSA, respiratory sinus arrhythmia.

TABLE 7 | Estimated marginal means for HR–DlPFC coupling during resting versus stressor phase across timescale and brain area.

		Resting		Stressor						
Brain area	**Timescale**	**Estimate**	**SE**	**Estimate**	**SE**	**Odds ratio**	**SE**	***Z***	***p***	***Adjusted p***
Left dlPFC	3–5 s	0.26	0.01	0.31	0.02	0.78	0.07	−2.58	0.010	0.049
	7–9 s	0.34	0.02	0.35	0.02	0.99	0.09	−0.09	0.929	0.929
	15–17 s	0.35	0.02	0.34	0.02	1.03	0.09	0.36	0.717	0.797
	31–33 s	0.45	0.02	0.36	0.02	1.43	0.13	4.11	<0.0001	<0.0001
	3–33 s	0.32	0.02	0.34	0.02	0.91	0.08	−0.99	0.321	0.478
Right dlPFC	3–5 s	0.26	0.01	0.3	0.02	0.82	0.08	−2.11	0.035	0.118
	7–9 s	0.33	0.02	0.35	0.02	0.91	0.08	−1.01	0.313	0.478
	15–17 s	0.34	0.02	0.36	0.02	0.92	0.08	−0.96	0.335	0.478
	31–33 s	0.38	0.02	0.37	0.02	1.05	0.09	0.53	0.594	0.742
	3–33 s	0.31	0.02	0.34	0.02	0.88	0.08	−1.42	0.157	0.392

Note: Adjusted *p* values were corrected for multiple comparison using Bonferroni–Holmes. Note that the coherence for the stressor phased was calculated across random 2-min segments of data in order for the comparison to the 2-min resting phase to be made.
Abbreviations: dlPFC, dorsolateral prefrontal cortex; HR, heart rate.

TABLE 8 | Estimated marginal means for RSA–DlPFC coupling during resting versus stressor phase across timescale and brain area.

		Resting		Stressor						
Brain area	**Timescale**	**Estimate**	**SE**	**Estimate**	**SE**	**Odds ratio**	**SE**	***Z***	***p***	***Adjusted p***
Left dlPFC	3–5 s	0.31	0.02	0.33	0.02	0.90	0.08	−1.17	0.243	0.347
	7–9 s	0.31	0.02	0.34	0.02	0.85	0.08	−1.81	0.071	0.142
	15–17 s	0.28	0.02	0.29	0.02	0.94	0.09	−0.61	0.544	0.544
	31–33 s	0.42	0.02	0.36	0.02	1.30	0.11	3.05	0.002	0.012
	3–33 s	0.33	0.02	0.34	0.02	0.93	0.08	−0.78	0.436	0.484
Right dlPFC	3–5 s	0.30	0.02	0.33	0.02	0.90	0.08	−1.21	0.227	0.347
	7–9 s	0.30	0.02	0.34	0.02	0.84	0.08	−1.93	0.054	0.135
	15–17 s	0.27	0.01	0.32	0.02	0.79	0.07	−2.49	0.013	0.042
	31–33 s	0.46	0.02	0.39	0.02	1.35	0.12	3.44	<0.0001	0.006
	3–33 s	0.33	0.02	0.35	0.02	0.92	0.08	−0.95	0.342	0.428

Note: Adjusted *p* values were corrected for multiple comparison using Bonferroni–Holmes. Note that the coherence for the stressor phased was calculated across random 2-min segments of data in order for the comparison to the 2-min resting phase to be made.
Abbreviations: dlPFC, dorsolateral prefrontal cortex; RSA, respiratory sinus arrhythmia.

TABLE 9 | Summary of results across cardiac measures and brain areas.

Cardiac measure	Side of dlPFC	True versus random during rest	True versus random during stress	Rest versus stress
HR	Left	True pairings higher in 4/5 timescales: **7–9 s, 15–17 s, 32–33 s, 3–33 s**	True pairings higher in 4/6 timescales: **15–17 s, 32–33 s, 63–65 s, 3–65 s**	Higher during stress in *3–5 s*, **31–33 s**
	Right	True pairings higher in 4/5 timescales: **7–9 s, 15–17 s, 32–33 s, 3–33 s**	True pairings higher in 4/6 timescales: **15–17 s, 32–33 s, 63–65 s, 3–65 s**	No differences
RSA	Left	True pairings higher in 3/5 timescales: *15–17 s*, **32–33 s, 3–33 s**	True pairings higher in 5/6 timescales: *7–9 s, 15–17 s*, **32–33 s, 63–65 s, 3–65 s**	Higher during rest in *31–33 s*
	Right	True pairings higher in 4/5 timescales: *7–9 s*, **15–17 s, 32–33 s, 3–33 s**	True pairings higher in 4/6 timescales: **15–17 s, 32–33 s, 63–65 s, 3–65 s**	Higher during stress in 15–17 s, higher during rest in *31–33 s*

Note: Italicized timescales indicate significant differences at $p < 0.05$, underline indicates $p < 0.01$, and bolded indicate $p < 0.001$.
Abbreviations: dlPFC, dorsolateral prefrontal cortex; HR, heart rate; RSA, respiratory sinus arrhythmia.

The coherence values were also compared between true and random pairings during the stressor phase for both HR– and RSA–dlPFC coherence (Models 2a and 2b; Tables 5 and 6). Pairing (*p*s < 0.001), Timescale ($p = 0.01$ for HR–dlPFC, $p < 0.001$ for RSA–dlPFC), and their interaction term (*p*s < 0.001) were all significant. Probing the estimated marginal means across brain area and timescale revealed that coupling was higher in true pairings for timescales greater than 7–9 s for both left and right dlPFC-HR coupling (*p*s < 0.001). For RSA signals, true coupling was greater than random coupling across timescales greater than 7 s for both the left and right dlPFC (*p*s < 0.05). The left dlPFC also exhibited significant coupling at the 7–9 s timescale (0.31 estimate for random pairing, 0.34 for true pairing; $Z(56) = 3.44$, $p = 0.038$). Regarding behavioral data, no significant effects were observed for any of the variables (child emotion dysregulation, the proportion of negative or positive affect) or Timescale × Affect/Emotion Dysregulation interactions for either HR– or RSA–dlPFC coherence during the stressor phase (Models 3a–5b).

When coupling across the two phases was compared (Models 5a and 5b; Tables 7 and 8), effects for Type were not significant (*p*s ≥ 0.19), while significant effects of Timescale (*p*s < 0.001) and the Timescale × Time interaction term (*p*s < 0.001) were found for both HR– and RSA–dlPFC coupling. Estimated marginal means revealed that coupling was greater at rest in the 31–33 s timescale for RSA–dlPFC across the right and left sides, with RSA–right dlPFC at rest having a mean coherence value 0.06 greater than that of the mean during stress ($Z(56) = 3.05$, $p = 0.012$), and RSA–left dlPFC at rest 0.07 greater than during stress ($Z(56) = 3.44$, $p = 0.006$). This trend was also observed for HR-left dlPFC coupling, where coherence values at rest were 0.09 higher than those during stress ($Z(56) = 4.11$, $p < 0.001$) at the 31–33 s timescale. During stress, HR–left dlPFC coupling was greater at shorter timescales of 3–5 s (*p*s = 0.049), and RSA–right dlPFC coupling was greater at the 15–17 s timescale for right dlPFC only ($Z(56) = -2.49$, $p = 0.042$).

Table 9 summarizes the observed significant differences in coupling between true and random pairings during rest and stress, as well as differences in coupling between phases.

4 | Discussion

This study is one of the first to investigate the temporal relations between PFC and ANS in young children. Paired-sample *t*-tests (Table 1) indicated significant phase-related increases in HR and decreases in RSA, providing evidence that the stressor phase successfully elicited an autonomic stress response. Using a multi-timescale analytic approach, coherence was observed between regulatory systems during restful and stressful conditions and at specific timescales. Stable coupling at rest may facilitate neurophysiological responsiveness to stress or challenge by enabling systems to adapt through quick neural and cardiac responsiveness divergence. The finding that the timescales at which coupling is observed differ between the resting and stressor phases supports the idea that coupling of physiological signals is sensitive to context and not a constant response or state. Moreover, both overly coupled, or coupling that persists across contexts, and decoupled neurophysiological systems may be maladaptive [74]. However, there was no relation with child positive or negative affect that may support such a relationship, which may be due to this study's relatively high-functioning community sample. Moreover, the present study's behavioral coding scheme captured only the expression of negative and positive affect and not the intensity of that expression, which may have inhibited the ability to detect a relationship. It is also possible that this study was underpowered to detect such an effect with a sample size of 55. Regardless, the finding that significant coupling varies by timescale affirms that the dlPFC and ANS interact temporally and are not just related to one another when examined across the entire task duration. The differences in patterns of significance in left and right dlPFC provide further support for lateralization of the dlPFC as it relates to the ANS and self-regulation. Moreover, this work provides support for the use of continuous wavelet coherence or other measures that allow for multiple timescales to be examined to measure ANS–dlPFC coupling, particularly when this coupling is examined during responses to stress or challenge.

The finding that dlPFC–HR coupling was significant only at timescales 15 s and longer (0.015–0.067 Hz) during the stressor

phase may suggest that PFC–ANS coupling is driven by changes in arterial stiffness that are related to both HR and cerebral blood flow. This frequency range captures portions of both the low (0.04−0.15 Hz) and very low frequency (0.0033−0.04 Hz) bands of HRV. Low-frequency HRV is thought to reflect sympathetic activity primarily related to baroreflex function [75]. The 0.021−0.05 Hz range of cardiovascular oscillations is associated with neurogenic activity of the vessel wall and vascular endothelial function, which are related to blood flow regulation in the nervous system [76]. Oscillations in the 0.052–0.145 Hz range of cardiovascular systems and fMRI have been specifically associated with myogenic activity, which captures changes in blood flow and blood oxygenation related to SNS control [76–78]. Importantly, fMRI connectivity in frontal cortical networks concentrates in ultra-low frequencies of 0.01–0.06 Hz and 0–0.08 Hz, suggesting that these timescales may better capture interactions across brain regions [79–81]. Connectivity in children has also been observed in these frequencies, with resting state connectivity concentrating primarily in the 0.01−0.05 Hz in infants 39−42 weeks old [82]. In children aged 6−10 years old, resting state connectivity is present across the 0−0.1 Hz range in various regions of the brain [83]. The concentration of connectivity in the same frequency bands as our observed coherence suggests that heart−brain coupling at these timescales may reflect neurovascular feedback during challenge.

However, very-low frequency oscillations also overlap with systemic physiology like Mayer waves, raising the possibility that the coherence observed in this study was driven by changes in the HbR concentrations due to systemic rather than neural mechanisms. However, as mentioned previously, oscillations in this range are also associated with neurovascular and cortical processes. Previous research has found that fNIRS-measured brain activity in these very-low frequency oscillations ceases after brain death, whereas activity at frequencies of systemic physiology (e.g., cardiac and respiratory rhythms) persists [84]. If systemic physiology were driving coherence, we would expect to see global increases in coherence values across both true and random pairings at timescales of respiration 0.2−0.3 Hz and Mayer waves around 0.1 Hz, consistent across task and brain area. Although we would not expect superficial coupling driven by systemic physiology to produce the specific pattern of differences in coherence in true versus random pairings across task, brain area, and timescale found in the present study, we cannot rule out systemic physiology as a driver of coupling, especially given that short-channel regression was not used in the present study, as its efficacy in young children had yet to be established when data was collected [85, 86].

Arterial stiffness and baroreflex activation may present as a mechanism through which the brain and heart interact in response to challenges that, while affected by respiration, would not be captured if only the frequency of respiration is examined regarding cardiac signals. These results suggest that stress prunes widespread dlPFC−HR coupling at rest down to rhythms related to changes in blood flow, possibly suggesting a baroreflex-dominated neurovascular feedback mechanism in the face of challenge [87]. Previous research with adults suggests that the PFC modifies baroreflex control in the face of stress [88] and that neural mechanisms are primarily responsible for acute changes in arterial blood pressure [89]. These possibilities introduce another potential reason for why coherence was not associated with positive or negative affectivity in the present study. Considering that the PFC, neurovascular coupling, and emotion regulation are not fully developed in early childhood [29, 82], it is possible that the relation between neurovascular coupling and emotion regulation does not emerge until later in development. Given the novelty of this study and the scant foundational work in this area, much more work is needed to understand the coupling, or lack thereof, between biological systems and behavior.

While only mean coherence values were considered in the current study, wavelet coherence analysis also contains information about phase differences between the two signals. Phase differences provide information about whether and to what degree one signal leads another at a specific frequency and are associated with the coherence values at that same frequency. Future work should explore the use of phase differences alongside coherence values to evaluate whether coupling occurs in a consistent positive or negative direction, and whether one signal leads the other, and to what degree, as this may provide further insight into how coupling is produced. Determining if coupling occurs in a positive or negative direction would better inform potential use and interpretation of RSA and low-frequency HR as biomarkers of cognitive control. Phase information could help determine whether coupling at timescales related to baroreflex is related to simultaneous response to arterial pressure changes or a neurovisceral integration channel distinct from vagal pathways. Additionally, a cross-frequency approach could be used to examine whether low and high frequencies of ANS and PFC are modulating one another within the regions of significant synchrony identified in the present study. Future work should also consider wavelet bispectra approaches that may be used to identify the presence of a third signal that is responsible for concurrent changes in HR and hemoglobin concentrations, such as blood pressure. Additionally, studies using fNIRS should also use short-channel regression to better filter out systemic physiological noise produced by scalp hemodynamics, as recent work has confirmed their efficacy in young children [86]. Studies should also consider collecting respiration and blood pressure data via tools such as respiration belt regressors and continuous noninvasive arterial pressure to better tease apart the interactions between brain activity, respiration, and cardiac physiology. Researchers who collect such data could consider employing partial wavelet coherence methods to determine whether coupling exists between HR and brain activity data when respiration and/or blood pressure is controlled for. Moreover, researchers who wish to use cardiac physiology to understand self-regulation may consider including both RSA and untransformed HR data when applicable to further probe differences in associations with these signals.

5 | Conclusion

In conclusion, this study's results show that the coupling of rhythms in the neural and cardiovascular systems reflects processes of self-regulation during early and middle childhood. Differences in coupling between restful and stressful periods suggest that changes in task and social conditions are associated with shifts in dynamical modes of self-regulation. Social con-

ditions for children are nurtured by interactions with mothers and caregivers, and future studies may investigate whether these interactions are associated with dyadic coupling between developing child and developed adult systems. Moreover, this study highlights the importance of considering timescales when examining such coupling and provides support for the use of wavelet coherence to do so.

Author Contributions

G.S. conceived of the project, conducted analyses, and wrote the manuscript. K.L. assisted in manuscript writing and editing. C.J.H. and A.O. assisted with manuscript editing. C.B. and D.G. assisted with data collection. C.J. assisted with manuscript editing, and data collection and processing. K.E.M. assisted with data collection and manuscript editing. C.S. and D.A. conceptualized the initial study, secured funding, and assisted with manuscript editing. D.H.A. and C.K. provided mentorship and assistance with conceptualization and editing.

Acknowledgments

We thank Bhumy Patel and Elizabeth Bravo for assistance with data collection and behavioral coding. This work was supported by the National Science Foundation grant DS-2314964 awarded to D.H.A.

Conflicts of Interest

All authors declare no actual or perceived conflicts of interest in the conducting or reporting of this research.

Data Availability Statement

Deidentified data and R code have been deposited on the Open Science Framework (https://osf.io/mqfbp) and are publicly available as of the publication date. Any additional information required to reanalyze the data reported in this paper is available from the lead contact upon request.

References

1. C. Blair and A. Ursache, "A Bidirectional Model of Executive Functions and Self-Regulation," in *Handbook of Self-Regulation: Research, Theory, and Applications*, 2nd ed., ed. K. D. Vohs and R. F. Baumeister (Guilford Press, 2011), 300–320.

2. W. A. Collins and S. D. Madsen, "Parenting During Middle Childhood," in *Handbook of Parenting*, ed. M. H. Bornstein (Routledge, 2019), 81–110.

3. J. J. Montroy, R. P. Bowles, L. E. Skibbe, M. M. McClelland, and F. J. Morrison, "The Development of Self-Regulation Across Early Childhood," *Developmental Psychology* 52, no. 11 (2016): 1744.

4. S. G. Peoples, E. L. Davis, and R. J. Brooker, "Variation in Coupling Across Neural and Cardiac Systems of Regulation Is Linked to Markers of Anxiety Risk in Preschool," *Development and Psychopathology* 37, no. 2 (2025): 766–778, https://doi.org/10.1017/S0954579424000609.

5. B. M. Appelhans and L. J. Luecken, "Heart Rate Variability as an Index of Regulated Emotional Responding," *Review of General Psychology* 10, no. 3 (2006): 229–240, https://doi.org/10.1037/1089-2680.10.3.229.

6. T. P. Beauchaine, "Respiratory Sinus Arrhythmia: A Transdiagnostic Biomarker of Emotion Dysregulation and Psychopathology," *Current Opinion in Psychology* 3 (2015): 43–47, https://doi.org/10.1016/j.copsyc.2015.01.017.

7. H. G. Kim, E. J. Cheon, D. S. Bai, Y. H. Lee, and B. H. Koo, "Stress and Heart Rate Variability: A Meta-Analysis and Review of the Literature," *Psychiatry Investigation* 15, no. 3 (2018): 235–245, https://doi.org/10.30773/pi.2017.08.17.

8. F. A. Koopman, S. P. Stoof, R. H. Straub, M. A. Van Maanen, M. J. Vervoordeldonk, and P. P. Tak, "Restoring the Balance of the Autonomic Nervous System as an Innovative Approach to the Treatment of Rheumatoid Arthritis," *Molecular Medicine* 17, no. 9–10 (2011): 937–948, https://doi.org/10.2119/molmed.2011.00065.

9. J. F. Thayer and R. D. Lane, "A Model of Neurovisceral Integration in Emotion Regulation and Dysregulation," *Journal of Affective Disorders* 61, no. 3 (2000): 201–216, https://doi.org/10.1016/s0165-0327(00)00338-4.

10. M. Sklerov, E. Dayan, and N. Browner, "Functional Neuroimaging of the Central Autonomic Network: Recent Developments and Clinical Implications," *Clinical Autonomic Research* 29, no. 6 (2019): 555–566.

11. J. M. Karemaker, "An Introduction Into Autonomic Nervous Function," *Physiological Measurement* 38, no. 5 (2017): R89.

12. J. P. Saul, "Beat-to-Beat Variations of Heart Rate Reflect Modulation of Cardiac Autonomic Outflow," *Physiology* 5, no. 1 (1990): 32–37.

13. S. W. Porges, "Polyvagal Theory: A Biobehavioral Journey to Sociality," *Comprehensive Psychoneuroendocrinology* 7 (2021): 100069.

14. J. A. Waxenbaum, V. Reddy, and M. A. Varacallo, "Anatomy, Autonomic Nervous System," *StatPearls [Internet]* (StatPearls Publishing, 2023).

15. D. Hering, K. Lachowska, and M. Schlaich, "Role of the Sympathetic Nervous System in Stress-Mediated Cardiovascular Disease," *Current Hypertension Reports* 17 (2015): 1–9, https://doi.org/10.1007/s11906-015-0594-5.

16. F. Shaffer and J. P. Ginsberg, "An Overview of Heart Rate Variability Metrics and Norms," *Frontiers in Public Health* 5 (2017): 258, https://doi.org/10.3389/fpubh.2017.00258.

17. S. W. Porges, "The Polyvagal Perspective," *Biological Psychology* 74, no. 2 (2007): 116–143, https://doi.org/10.1016/j.biopsycho.2006.06.009.

18. S. Porges, *The Polyvagal Theory: Neurophysiological Foundations of Emotions, Attachment, Communication, and Self-Regulation* (W.W. Norton, 2011).

19. L. R. Sacrey, S. Raza, V. Armstrong, et al., "Physiological Measurement of Emotion From Infancy to Preschool: A Systematic Review and Meta-Analysis," *Brain and Behavior* 11, no. 2 (2021): e01989, https://doi.org/10.1002/brb3.1989.

20. N. J. Kelley, A. Gallucci, P. Riva, L. J. Romero Lauro, and B. J. Schmeichel, "Stimulating Self-Regulation: A Review of Non-Invasive Brain Stimulation Studies of Goal-Directed Behavior," *Frontiers in Behavioral Neuroscience* 12 (2019): 337, https://doi.org/10.3389/fnbeh.2018.00337.

21. C. S. Li and R. Sinha, "Inhibitory Control and Emotional Stress Regulation: Neuroimaging Evidence for Frontal-Limbic Dysfunction in Psycho-Stimulant Addiction," *Neuroscience and Biobehavioral Reviews* 32, no. 3 (2008): 581–597, https://doi.org/10.1016/j.neubiorev.2007.10.003.

22. D. T. Stuss, "Biological and Psychological Development of Executive Functions," *Brain and Cognition* 20, no. 1 (1992): 8–23, https://doi.org/10.1016/0278-2626(92)90059-u.

23. J. Lévesque, Y. Joanette, B. Mensour, et al., "Neural Basis of Emotional Self-Regulation in Childhood," *Neuroscience* 129, no. 2 (2004): 361–369, https://doi.org/10.1016/j.neuroscience.2004.07.032.

24. D. A. Fair, A. L. Cohen, J. D. Power, et al., "Functional Brain Networks Develop From a "Local to Distributed" Organization," *PLoS Computational Biology* 5, no. 5 (2009): e1000381, https://doi.org/10.1371/journal.pcbi.1000381.

25. V. Menon and M. D'Esposito, "The Role of PFC Networks in Cognitive Control and Executive Function," *Neuropsychopharmacology* 47, no. 1 (2022): 90–103.

26. C. M. Eng, R. J. Vargas, H. L. Fung, et al., "Prefrontal Cortex Intrinsic Functional Connectivity and Executive Function in Early Childhood and

Early Adulthood Using fNIRS," *Developmental Cognitive Neuroscience* 74 (2025): 101570, https://doi.org/10.1016/j.dcn.2025.101570.

27. Ö. E. Demir-Lira, J. L. Voss, J. T. O'Neil, M. J. Briggs-Gowan, L. S. Wakschlag, and J. R. Booth, "Early-Life Stress Exposure Associated With Altered Prefrontal Resting-State fMRI Connectivity in Young Children," *Developmental Cognitive Neuroscience* 19 (2016): 107–114, https://doi.org/10.1016/j.dcn.2016.02.003.

28. A. T. Park, J. A. Leonard, P. K. Saxler, A. B. Cyr, J. D. E. Gabrieli, and A. P. Mackey, "Amygdala-Medial Prefrontal Cortex Connectivity Relates to Stress and Mental Health in Early Childhood," *Social Cognitive and Affective Neuroscience* 13, no. 4 (2018): 430–439, https://doi.org/10.1093/scan/nsy017.

29. A. S. Grabell, T. J. Huppert, F. A. Fishburn, et al., "Neural Correlates of Early Deliberate Emotion Regulation: Young Children's Responses to Interpersonal Scaffolding," *Developmental Cognitive Neuroscience* 40 (2019): 100708, https://doi.org/10.1016/j.dcn.2019.100708.

30. M. I. Posner and M. K. Rothbart, "Attention, Self-Regulation and Consciousness," *Philosophical Transactions of the Royal Society of London Series B, Biological Sciences* 353, no. 1377 (1998): 1915–1927, https://doi.org/10.1098/rstb.1998.0344.

31. S. Tsujimoto, "The Prefrontal Cortex: Functional Neural Development During Early Childhood," *Neuroscientist* 14, no. 4 (2008): 345–358, https://doi.org/10.1177/1073858408316002.

32. S. E. Gathercole, S. J. Pickering, B. Ambridge, and H. Wearing, "The Structure of Working Memory From 4 to 15 Years of Age," *Developmental Psychology* 40, no. 2 (2004): 177–190, https://doi.org/10.1037/0012-1649.40.2.177.

33. M. C. Davidson, D. Amso, L. C. Anderson, and A. Diamond, "Development of Cognitive Control and Executive Functions From 4 to 13 Years: Evidence From Manipulations of Memory, Inhibition, and Task Switching," *Neuropsychologia* 44, no. 11 (2006): 2037–2078, https://doi.org/10.1016/j.neuropsychologia.2006.02.006.

34. A. Diamond, "Normal Development of Prefrontal Cortex From Birth to Young Adulthood: Cognitive Functions, Anatomy, and Biochemistry," in *Principles of Frontal Lobe Function*, ed. D. T. Stuss and R. T. Knight (Oxford University Press, 2002), 466–503, https://doi.org/10.1093/acprof:oso/9780195134971.003.0029.

35. M. Huizinga, C. V. Dolan, and M. W. van der Molen, "Age-Related Change in Executive Function: Developmental Trends and a Latent Variable Analysis," *Neuropsychologia* 44, no. 11 (2006): 2017–2036, https://doi.org/10.1016/j.neuropsychologia.2006.01.010.

36. K. Rubia, A. B. Smith, M. J. Brammer, and E. Taylor, "Right Inferior Prefrontal Cortex Mediates Response Inhibition While Mesial Prefrontal Cortex Is Responsible for Error Detection," *Neuroimage* 20, no. 1 (2003): 351–358, https://doi.org/10.1016/s1053-8119(03)00275-1.

37. B. R. Williams, J. S. Ponesse, R. J. Schachar, G. D. Logan, and R. Tannock, "Development of Inhibitory Control Across the Life Span," *Developmental Psychology* 35, no. 1 (1999): 205.

38. Sameroff, A. J., & Haith, M. M., *The Five to Seven Year Shift: The Age of Reason and Responsibility* (University of Chicago Press, 1996).

39. M. Del Giudice, B. J. Ellis, and E. A. Shirtcliff, "The Adaptive Calibration Model of Stress Responsivity," *Neuroscience and Biobehavioral Reviews* 35, no. 7 (2011): 1562–1592, https://doi.org/10.1016/j.neubiorev.2010.11.007.

40. J. G. Kerns, "Anterior Cingulate and Prefrontal Cortex Activity in an FMRI Study of Trial-to-Trial Adjustments on the Simon Task," *Neuroimage* 33, no. 1 (2006): 399–405, https://doi.org/10.1016/j.neuroimage.2006.06.012.

41. A. F. Arnsten, "Stress Signalling Pathways That Impair Prefrontal Cortex Structure and Function," *Nature Reviews Neuroscience* 10, no. 6 (2009): 410–422, https://doi.org/10.1038/nrn2648.

42. E. A. Boschin, M. M. Brkic, J. S. Simons, and M. J. Buckley, "Distinct Roles for the Anterior Cingulate and Dorsolateral Prefrontal Cortices During Conflict Between Abstract Rules," *Cerebral Cortex* 27, no. 1 (2017): 34–45, https://doi.org/10.1093/cercor/bhw350.

43. O. Mohamed Ali, M. R. J. Vandermeer, P. Liu, M. F. Joanisse, D. M. Barch, and E. P. Hayden, "Associations Between Childhood Irritability and Neural Reactivity to Maternal Feedback in Adolescence," *Biological Psychology* 182 (2023): 108645, https://doi.org/10.1016/j.biopsycho.2023.108645.

44. M. Achterberg, A. C. K. van Duijvenvoorde, M. H. van IJzendoorn, M. J. Bakermans-Kranenburg, and E. A. Crone, "Longitudinal Changes in DLPFC Activation During Childhood Are Related to Decreased Aggression Following Social Rejection," *Proceedings of the National Academy of Sciences of the United States of America* 117, no. 15 (2020): 8602–8610, https://doi.org/10.1073/pnas.1915124117.

45. L. D. Godoy, M. T. Rossignoli, P. Delfino-Pereira, N. Garcia-Cairasco, and E. H. de Lima Umeoka, "A Comprehensive Overview on Stress Neurobiology: Basic Concepts and Clinical Implications," *Frontiers in Behavioral Neuroscience* 12 (2018): 127, https://doi.org/10.3389/fnbeh.2018.00127.

46. J. F. Thayer, F. Ahs, M. Fredrikson, J. J. Sollers, 3rd, and T. D. Wager, "A Meta-Analysis of Heart Rate Variability and Neuroimaging Studies: Implications for Heart Rate Variability as a Marker of Stress and Health," *Neuroscience and Biobehavioral Reviews* 36, no. 2 (2012): 747–756, https://doi.org/10.1016/j.neubiorev.2011.11.009.

47. T. A. Iseger, M. Arns, J. Downar, D. M. Blumberger, Z. J. Daskalakis, and F. Vila-Rodriguez, "Cardiovascular Differences Between Sham and Active iTBS Related to Treatment Response in MDD," *Brain Stimulation* 13, no. 1 (2020): 167–174, https://doi.org/10.1016/j.brs.2019.09.016.

48. Y. Wang, M. K. Hensley, A. Tasman, L. Sears, M. F. Casanova, and E. M. Sokhadze, "Heart Rate Variability and Skin Conductance During Repetitive TMS Course in Children With Autism," *Applied Psychophysiology and Biofeedback* 41, no. 1 (2016): 47–60, https://doi.org/10.1007/s10484-015-9311-z.

49. T. Nguyen, S. Hoehl, B. I. Bertenthal, and D. H. Abney, "Coupling Between Prefrontal Brain Activity and Respiratory Sinus Arrhythmia in Infants and Adults," *Developmental Cognitive Neuroscience* 53 (2022): 101047, https://doi.org/10.1016/j.dcn.2021.101047.

50. A. Grinsted, J. C. Moore, and S. Jevrejeva, "Application of the Cross Wavelet Transform and Wavelet Coherence to Geophysical Time Series," *Nonlinear Processes Geophysics* 11 (2004): 561–566, https://doi.org/10.5194/npg-11-561-2004.

51. P. Grossman, "Respiratory Sinus Arrhythmia (RSA), Vagal Tone and Biobehavioral Integration: Beyond Parasympathetic Function," *Biological Psychology* 186 (2024): 108739, https://doi.org/10.1016/j.biopsycho.2023.108739.

52. A. Sanchez-Lopez, M. A. Vanderhasselt, J. Allaert, C. Baeken, and R. De Raedt, "Neurocognitive Mechanisms Behind Emotional Attention: Inverse Effects of Anodal tDCS Over the Left and Right DLPFC on Gaze Disengagement From Emotional Faces," *Cognitive, Affective, & Behavioral Neuroscience* 18 (2018): 485–494, https://doi.org/10.3758/s13415-018-0582-8.

53. L. K. White, W. Makhoul, M. Teferi, Y. I. Sheline, and N. L. Balderston, "The Role of dlPFC Laterality in the Expression and Regulation of Anxiety," *Neuropharmacology* 224 (2023): 109355, https://doi.org/10.1016/j.neuropharm.2022.109355.

54. M. R. Gunnar, N. M. Talge, and A. Herrera, "Stressor Paradigms in Developmental Studies: What Does and Does Not Work to Produce Mean Increases in Salivary Cortisol," *Psychoneuroendocrinology* 34, no. 7 (2009): 953–967, https://doi.org/10.1016/j.psyneuen.2009.02.010.

55. K. R. Kryski, H. J. Smith, H. I. Sheikh, S. M. Singh, and E. P. Hayden, "Assessing Stress Reactivity Indexed via Salivary Cortisol in Preschool-Aged Children," *Psychoneuroendocrinology* 36, no. 8 (2011): 1127–1136, https://doi.org/10.1016/j.psyneuen.2011.02.003.

56. E. Lunkenheimer, C. J. Kemp, R. G. Lucas-Thompson, P. M. Cole, and E. C. Albrecht, "Assessing Biobehavioural Self-Regulation and Coregula-

tion in Early Childhood: The Parent-Child Challenge Task," *Infant and Child Development* 26, no. 1 (2017): e1965, https://doi.org/10.1002/icd.1965.

57. M. E. Hale, K. E. Morrow, A. M. George, A. Gayer, M. O. Caughy, and C. Suveg, "Maternal Negative Affect Moderates Behavioral and Physiological Synchrony in Latinx and Black Mother-Child Dyads," *Developmental Psychobiology* 65, no. 5 (2023): e22394, https://doi.org/10.1002/dev.22394.

58. A. M. George, M. E. Hale, H. Wang, D. Abney, M. O. Caughy, and C. Suveg, "Child Self-Regulation Profiles Relate to Emotion Parenting in Black and Latinx Mother-Child Dyads," *Journal of Applied Developmental Psychology* 95 (2024): 101708, https://doi.org/10.1016/j.appdev.2024.101708.

59. L. A. Wallis, M. Healy, M. B. Undy, and I. Maconochie, "Age Related Reference Ranges for Respiration Rate and Heart Rate From 4 to 16 Years," *Archives of Disease in Childhood* 90, no. 11 (2005): 1117–1121, https://doi.org/10.1136/adc.2004.068718.

60. J. M. Dollar, S. D. Calkins, N. T. Berry, et al., "Developmental Patterns of Respiratory Sinus Arrhythmia From Toddlerhood to Adolescence," *Developmental Psychology* 56, no. 4 (2020): 783–794, https://doi.org/10.1037/dev0000894.

61. H. K. Lackner, M. T. W. Eglmaier, S. Hackl-Wimmer, et al., "How to Use Heart Rate Variability: Quantification of Vagal Activity in Toddlers and Adults in Long-Term ECG," *Sensors* 20, no. 20 (2020): 5959, https://doi.org/10.3390/s20205959.

62. E. J. Kiel and E. M. Aaron, "Respiratory Sinus Arrhythmia, Effortful Control, and Child Social Anxiety Symptoms," *Research on Child and Adolescent Psychopathology* 52, no. 9 (2024): 1441–1453, https://doi.org/10.1007/s10802-024-01202-z.

63. D. H. Abney, E. B. daSilva, G. F. Lewis, and B. I. Bertenthal, "A Method for Measuring Dynamic Respiratory Sinus Arrhythmia (RSA) in Infants and Mothers," *Infant Behavior and Development* 63 (2021): 101569, https://doi.org/10.1016/j.infbeh.2021.101569.

64. T. J. Huppert, S. G. Diamond, M. A. Franceschini, and D. A. Boas, "HomER: A Review of Time-Series Analysis Methods for Near-Infrared Spectroscopy of the Brain," *Applied Optics* 48, no. 10 (2009): D280–D298.

65. T. J. Huppert, HOMER3: NIRS Processing Package [Computer software] (2023), https://github.com/BUNPC/Homer3.

66. E. Kirilina, N. Yu, A. Jelzow, H. Wabnitz, A. M. Jacobs, and I. Tachtsidis, "Identifying and Quantifying Main Components of Physiological Noise in Functional Near Infrared Spectroscopy on the Prefrontal Cortex," *Frontiers in Human Neuroscience* 7 (2013): 864.

67. E. A. Piazza, L. Hasenfratz, U. Hasson, and C. Lew-Williams, "Infant and Adult Brains Are Coupled to the Dynamics of Natural Communication," *Psychological Science* 31, no. 1 (2020): 6–17, https://doi.org/10.1177/0956797619878698.

68. M. T. Owen, J. Klausli, and M. Murrey, *The NICHD Study of Early Child Care and Youth Development Parent-Child Interaction Scales: Middle Childhood* (University of Texas at Dallas, 2000).

69. A. Shields and D. Cicchetti, "Emotion Regulation Among School-Age Children: The Development and Validation of a New Criterion Q-Sort Scale," *Developmental Psychology* 33, no. 6 (1997): 906–916, https://doi.org/10.1037/0012-1649.33.6.906.

70. T. Gouhier, A. Grinsted, and V. Simko, *R package biwavelet: Conduct Univariate and Bivariate Wavelet Analyses*. (Version 0.20.22) (2024), https://github.com/tgouhier/biwavelet.

71. J. Issartel, T. Bardainne, P. Gaillot, and L. Marin, "The Relevance of the Cross-Wavelet Transform in the Analysis of Human Interaction–A Tutorial," *Frontiers in Psychology* 5 (2015): 1566.

72. M. McGillycuddy, D. I. Warton, G. Popovic, et al., "Parsimoniously Fitting Large Multivariate Random Effects in glmmTMB," *Journal of Statistical Software* 112, no. 1 (2025): 1–19, https://doi.org/10.18637/jss.v112.i01.

73. R. Lenth, emmeans: Estimated Marginal Means, Aka Least-Square Means. R-package version 1.10.6–090002 (2024), https://rvlenth.github.io/emmeans/.

74. M. L. Heltberg, S. Krishna, L. P. Kadanoff, and M. H. Jensen, "A Tale of Two Rhythms: Locked Clocks and Chaos in Biology," *Cell Systems* 12, no. 4 (2021): 291–303, https://doi.org/10.1016/j.cels.2021.03.003.

75. D. S. Goldstein, O. Bentho, M.-Y. Park, and Y. Sharabi, "Low-Frequency Power of Heart Rate Variability Is Not a Measure of Cardiac Sympathetic Tone but May be a Measure of Modulation of Cardiac Autonomic Outflows by Baroreflexes," *Experimental Physiology* 96, no. 12 (2011): 1255–1261, https://doi.org/10.1113/expphysiol.2010.056259.

76. A. Stefanovska, "Coupled Oscillators: Complex but Not Complicated Cardiovascular and Brain Interactions," *IEEE Engineering in Medicine and Biology Magazine* 26, no. 6 (2007): 25–29, https://doi.org/10.1109/emb.2007.907088.

77. F. Bajrović, M. Čenčur, M. Hožič, S. Ribarič, and A. Stefanovska, "The Contribution of Lumbar Sympathetic Neurones Activity to Rat's Skin Blood Flow Oscillations," *Pflügers Archiv—European Journal of Physiology* 439, no. 7 (2000): R158–R160, https://doi.org/10.1007/BF03376556.

78. B. Biswal, F. Z. Yetkin, V. M. Haughton, and J. S. Hyde, "Functional Connectivity in the Motor Cortex of Resting Human Brain Using Echo-Planar MRI," *Magnetic Resonance in Medicine* 34 (1995): 537–541, https://doi.org/10.1002/mrm.1910340409.

79. C. W. Wu, H. Gu, H. Lu, E. A. Stein, J. H. Chen, and Y. Yang, "Frequency Specificity of Functional Connectivity in Brain Networks," *Neuroimage* 42, no. 3 (2008): 1047–1055, https://doi.org/10.1016/j.neuroimage.2008.05.035.

80. S. Achard, R. Salvador, B. Whitcher, J. Suckling, and E. Bullmore, "A Resilient, Low-Frequency, Small-World Human Brain Functional Network With Highly Connected Association Cortical Hubs," *Journal of Neuroscience* 26, no. 1 (2006): 63–72, https://doi.org/10.1523/JNEUROSCI.3874-05.2006.

81. R. Salvador, A. Martínez, E. Pomarol-Clotet, et al., "A Simple View of the Brain Through a Frequency-Specific Functional Connectivity Measure," *Neuroimage* 39, no. 1 (2008): 279–289, https://doi.org/10.1016/j.neuroimage.2007.08.018.

82. P. Fransson, B. Skiöld, S. Horsch, et al., "Resting-State Networks in the Infant Brain," *Proceedings of the National Academy of Sciences of the United States of America* 104, no. 39 (2007): 15531–15536, https://doi.org/10.1073/pnas.0704380104.

83. R. L. Muetzel, L. M. Blanken, S. Thijssen, et al., "Resting-State Networks in 6-to-10 Year Old Children," *Human Brain Mapping* 37, no. 12 (2016): 4286–4300, https://doi.org/10.1002/hbm.23309.

84. S. Schulthess, S. Friedl, G. Narula, et al., "Low Frequency Oscillations Reflect Neurovascular Coupling and Disappear After Cerebral Death," *Scientific Reports* 14, no. 1 (2024): 11287, https://doi.org/10.1038/s41598-024-61819-4.

85. P. Pinti, L. M. Dina, and T. J. Smith, "Ecological Functional Near-Infrared Spectroscopy in Mobile Children: Using Short Separation Channels to Correct for Systemic Contamination During Naturalistic Neuroimaging," *Neurophotonics* 11, no. 4 (2024): 045004, https://doi.org/10.1117/1.NPh.11.4.045004.

86. M. K. Yeung, "An Optical Window Into Brain Function in Children and Adolescents: A Systematic Review of Functional Near-Infrared Spectroscopy Studies," *Neuroimage* 227 (2021): 117672, https://doi.org/10.1016/j.neuroimage.2020.117672.

87. P. J. Gianaros, I. C. Onyewuenyi, L. K. Sheu, I. C. Christie, and H. D. Critchley, "Brain Systems for Baroreflex Suppression During Stress in Humans," *Human Brain Mapping* 33, no. 7 (2012): 1700–1716, https://doi.org/10.1002/hbm.21315.

88. D. C. Lagatta, A. Fassini, A. L. Terzian, F. M. A. Corrêa, and L. B. M. Resstel, "The Medial Prefrontal Cortex and the Cardiac Baroreflex

Activity: Physiological and Pathological Implications," *Pflugers Archiv: European Journal of Physiology* 475, no. 3 (2023): 291–307, https://doi.org/10.1007/s00424-022-02786-5.

89. P. A. Lanfranchi and V. K. Somers, "Arterial Baroreflex Function and Cardiovascular Variability: Interactions and Implications," *American Journal of Physiology Regulatory, Integrative and Comparative Physiology* 283, no. 4 (2002): R815–R826, https://doi.org/10.1152/ajpregu.00051.2002.

Supporting Information

Additional supporting information can be found online in the Supporting Information section.

Supplementary Tables: nyas70203-sup-001-SuppMat.docx